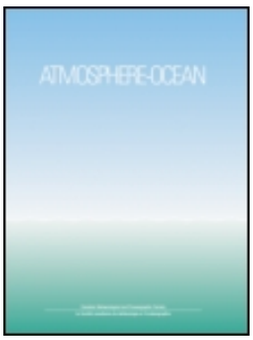

Atmosphere-Ocean

ISSN: 0705-5900 (Print) 1480-9214 (Online) Journal homepage: https://www.tandfonline.com/loi/tato20

Typhoon-Induced Variability of the Oceanic Surface Mixed Layer Observed by Argo Floats in the Western North Pacific Ocean

Qiaoyan Wu & Dake Chen

To cite this article: Qiaoyan Wu & Dake Chen (2012) Typhoon-Induced Variability of the Oceanic Surface Mixed Layer Observed by Argo Floats in the Western North Pacific Ocean, Atmosphere-Ocean, 50:sup1, 4-14, DOI: 10.1080/07055900.2012.712913

To link to this article: https://doi.org/10.1080/07055900.2012.712913

Typhoon-Induced Variability of the Oceanic Surface Mixed Layer Observed by Argo Floats in the Western North Pacific Ocean

Qiaoyan Wu[1,2,*] and Dake Chen[1,2,3]

[1]*State Key Laboratory of Satellite Ocean Environment Dynamics, Second Institute of Oceanography, Hangzhou, Zhejiang, China*
[2]*Department of Ocean Science and Engineering, Zhejiang University, Hangzhou, Zhejiang, China*
[3]*Lamont-Doherty Earth Observatory, Columbia University, New York, New York*

[Original manuscript received 2 March 2011; accepted 1 January 2012]

ABSTRACT *This study takes advantage of the newly established observational network of Argo floats to investigate the variability of the oceanic surface mixed layer (ML) in response to typhoons occurring over the period 2000–08 in the western North Pacific Ocean. After removing the background variability due to the seasonal cycle, the regionally averaged ML response is statistically analyzed as a function of the distance from the typhoon centre, the time after typhoon passage, the geographic location, the translation speed of the typhoon and the pre-existing patterns of oceanic circulation. Based on an unprecedented amount of new observational data, our analysis reveals some notable differences between ML temperature and ML depth changes induced by a typhoon, including the delayed response of ML temperature relative to ML depth, the longer restoring time of ML temperature, and the tendency of pre-existing cold-core features to favour ML cooling while warm-core features favour ML deepening.*

RÉSUMÉ *[Traduit par la rédaction] La présente étude tire profit du nouveau réseau de balises d'observation Argo qui étudie la variabilité de la couche de mélange de la surface océanique en réponse aux typhons survenus durant la période 2000–2008 dans l'ouest du Pacifique Nord. Après avoir éliminé la variabilité de fond due au cycle saisonnier, nous faisons une analyse statistique de la réponse de la couche de mélange, moyennée dans une région, en fonction de la distance du centre du typhon, du temps écoulé depuis le passage du typhon, du lieu géographique, de la vitesse de déplacement du typhon et des configurations de circulation océanique préexistantes. En se basant sur une quantité sans précédent de nouvelles données d'observation, notre analyse révèle des différences notables entre les changements de température et de profondeur de la couche de mélange produits par le typhon, y compris la réponse retardée de la température de la couche de mélange par rapport à la profondeur de la couche de mélange, le temps de rétablissement plus long de la température de la couche de mélange et la tendance des caractéristiques de noyaux froids préexistantes à favoriser le refroidissement de la couche de mélange pendant que les caractéristiques de noyaux chauds favorisent l'approfondissement de la couche de mélange.*

KEYWORDS ocean mixed layer; typhoon; Argo floats; statistical analysis

1 Introduction

The upper ocean response to the strong swirling forcing of typhoons has been a topic of both great scientific interest and practical importance. Many observational and modelling studies have shown that the response is often characterized by a rapid cooling of sea surface temperatures (SST) in the wake of a typhoon, ranging from 1° to 9°C (e.g., Price, 1981; Stramma et al., 1986; Lin et al., 2003; Walker et al., 2005). Typhoon-forced SST cooling is generally thought to be a result of vertical entrainment of deep cold water into the surface mixed layer (ML), whereas direct air–sea heat exchanges are considered to play a relatively minor role (Price, 1981; Emanuel, 1999).

The lack of subsurface observations has long been a major hindrance to understanding the interaction between the ocean and typhoons. Thanks to the increasing number of Argo profiling floats deployed in the world's oceans over the past decades (Roemmich et al., 2004; Gould, 2005), we can now observe the oceanic response to tropical cyclones on a global scale. Argo floats have no problem operating under the harsh conditions brought about by typhoons, and they measure both temperature and salinity, thus providing a

*Corresponding author's email: qwu@sio.org.cn

complete picture of the structure of the upper ocean and its variability in response to typhoons. The past decade has seen increasingly significant contributions of Argo data to our understanding of the oceanic role in regulating typhoon intensity (e.g., Lin et al., 2008, 2009; Siswanto et al., 2008).

Despite the potential of Argo data for studying the oceanic response to typhoons, we should be cautious in our interpretation of Argo data. The changes in thermohaline structure recorded by Argo profiles may come from other oceanic processes, such as internal waves, eddies, frontal movements, as well as seasonal variations. For example, Iwasaka et al. (2006) revealed the seasonal evolution of the ML in the western North Pacific Ocean by following an Argo float for more than nine months. When using Argo profiles to study ML variations associated with the passage of a typhoon, the background seasonal variability contained in the observations should be taken into account, especially at higher latitudes where such variability is pronounced.

In the western North Pacific Ocean, abundant warm and cold mesoscale features are observed all year round. Many of these mesoscale features are associated with the Kuroshio rings (Yasuda et al., 1992) or are a result of the instability of the shear flow between the westward North Equatorial Current and the eastward Subtropical Countercurrent (Qiu, 1999; Roemmich & Gilson, 2001). In a recent study, Jaimes et al. (2011) found that an upwelling (downwelling) regime prevails under a tropical cyclone's eye as it translates over cold (warm) mesoscale features. It has been suggested that the mesoscale features are a critical condition for typhoon intensification (Lin et al., 2008) and are important for accurately simulating the ML cooling induced by tropical cyclones (Jaimes et al., 2011). Using Argo profiles to study the response of the upper ocean to typhoons must take into account the influence of these features.

In addition to the pre-existing ocean circulation patterns, it has been suggested that the oceanic response to typhoons is also a function of the intensity and translation speed of the typhoon and of the initial ML depth (Price, 1981; Walker et al., 2005; Zheng et al., 2008; Wada et al., 2009). These suggestions were mostly based on case studies, and the relationship between these factors and the ML variability have not been fully investigated in a statistical manner. Based on Argo observations from early years, Park et al. (2005) and Liu et al. (2007) analyzed the oceanic response to typhoons and demonstrated the application of Argo data for such analysis.

In this study, we take advantage of tens of thousands of Argo profiles in the western North Pacific Ocean from 2000 to 2008 to re-examine the response of the upper ocean to typhoons, as a function of the distance from the typhoon centre, the time after the typhoon passage, the geographic location, the translation speed of the typhoon, and the pre-existing ocean circulation patterns with the seasonal background variability removed. Our analysis differs from previous studies not only in the increased amount of Argo data used but also in the more complete set of parameters to be explored. We begin with a brief introduction of the observational data used for the study, followed by a validation of Argo observations for typhoon impact studies. Then we discuss the background ML variability in the western North Pacific Ocean and describe the ML response to typhoons as a function of different parameters.

2 Data processing

a Data

Typhoon data used in this study are the best track data from the Japan Meteorological Agency (JMA) spanning the period 2000 to 2008, and include the name, analysis time, centre location, 10-minute maximum sustained wind speed and central pressure of each typhoon. The translation speed of a typhoon is calculated according to the location of the typhoon centre at 6-hour intervals. Unless otherwise noted, in this study we will only consider northwestern Pacific Ocean tropical cyclones with a maximum sustained wind speed greater than 33 m s^{-1}; such cyclones are in the typhoon category.

All of the Argo data used here were provided by the China Argo Real-time Data Center (http://www.argo.org.cn/). Because Argo data are subject to biases in reported pressures, we limit our use of data to those with a quality control flag equal to one. In order to examine the ML change without the impact of a typhoon, we first created a dataset that consists of Argo profiles 500 km away from the typhoon centre and 20 days after the passage of the typhoon. The data in the non-passage areas were defined as background data (Wada & Chan, 2008). The background ML variability was simply measured as the difference between two successive profiles (with a 7–10 day recurring cycle). To evaluate the ML response to a typhoon, an Argo profile taken after the passage of a typhoon is paired with another profile taken before the passage of the typhoon to represent the variation induced by the typhoon. The maximum distance between the pair is restricted to 50 km. This scale selection is based on a trade-off between the data availability and the need to use data points as close as possible to estimate local response. Our preliminary tests indicate that our analysis results are not particularly sensitive to this criterion as long as it is in a reasonable range.

Sea surface height anomalies (SSHA) used in this study are from the merged product derived from the TOPography Experiment/Poseidon (TOPEX/Poseidon) satellite, Jason-1/2, the European Remote-Sensing Satellite-2 (ERS-2), Envisat and the GEOSAT Follow-On (GFO) satellite, provided by Archiving, Validation and Interpretation of Satellite Oceanographic data (Aviso; www.aviso.oceanobs.com) with a spatial resolution of 1/3° by 1/3° on a Mercator grid and a temporal resolution of seven days. The SSHA data used to evaluate the impact of initial oceanic conditions are within 30 km of the Argo profiles and within seven days before the typhoon passage. According to previous studies (Fu et al., 1994; Qiu, 1999; Shay et al., 2000; Lin et al., 2008), an

area-averaged SSHA feature greater (less) than 6 cm (−6 cm) is defined as a positive (negative) condition, while those in between are defined as neutral conditions.

b ML Criterion

Because Argo floats have very limited records in the upper 10 m, we define the surface mixed layer depth (MLD) as the depth where the temperature has decreased by 0.2°C from that at 10 m, following de Boyer Montégut et al. (2004). Choosing the 10 m depth as the reference level also avoids the diurnal variations in the first few metres in the ocean. Because Argo floats do not sample the upper 5 m of the ocean, the temperature above 10 m is assumed to be uniform (Grodsky et al., 2008). It is possible that such a treatment could underestimate surface temperature variability, but this may not be a serious limitation here because of the strong forcing of the typhoon. The mixed layer temperature (MLT) is calculated as the vertically averaged temperature above the base of the ML using trapezoidal numerical integration.

In principle, the MLD should be calculated based on density stratification, but in practice many different criteria have been used, also summarized by de Boyer Montégut et al. (2004). In that article they actually demonstrated that a 0.2°C temperature difference from that at the 10 m depth (the criterion used here) is the most appropriate for MLD estimation from individual profiles on a global scale. The effect of salinity was also evaluated by de Boyer Montégut et al. (2004, 2007) who concluded that in regions where a barrier layer exists, a density-based criterion is probably needed. Because our focus is on typhoons with wind speeds greater than 33 m s^{-1}, which mostly occur in the western North Pacific Ocean from 10°N to 45°N, our study area is thus not located where significant barrier layers form (Fig. 3 of de Boyer Montégut et al., 2007), and the temperature-based criterion is applicable.

3 Validity of Argo observations for a typhoon impact study

Although Argo floats were not designed to observe transient and synoptic phenomena, they are, nonetheless, useful for studying the oceanic response to typhoons despite their relatively low sampling rate. The reason is that the impact of typhoons has a lasting effect, and the restoration of the ocean to its pre-storm condition may take a long time (Withee & Johnson, 1976; Park et al., 2005); this makes it possible to use the float's repeating cycle of 7–10 days to measure the changes in the upper ocean induced by typhoons. More importantly, in areas where the distribution of Argo floats is relatively dense, such as the western North Pacific Ocean, the availability of Argo profiles for a translating cyclone is actually much higher than that expected from an individual float. In this study, our focus is on regionally averaged ML response to typhoons rather than on individual events. As long as the total sample size is large enough, the estimated mean response should be statistically significant.

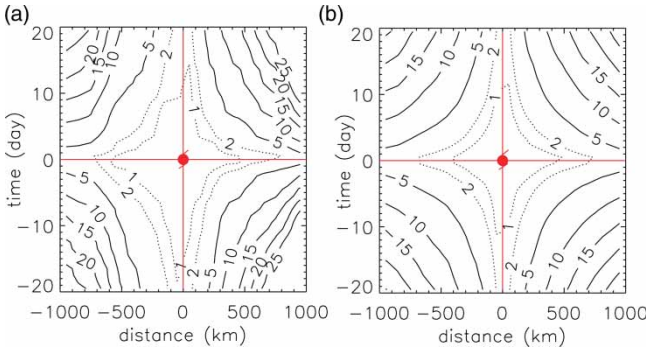

Fig. 1 Average number of Argo profiles per day available in the western North Pacific Ocean for a tropical cyclone as a function of distance from the cyclone centre and time before and after the cyclone passage. The calculation is based on (a) typhoons and (b) all tropical cyclones, respectively.

As an example, Fig. 1a shows the average number of Argo profiles per day available in the western North Pacific Ocean for a typhoon occurring in 2008 as a function of time and distance from the typhoon centre. As expected, the larger the time and space windows chosen, the more profiles that are available. Typically there is at least one profile within a time-space window that spans 200 km on either side of the typhoon centre and 2.5 days either before or after the passage of the typhoon, as indicated by the inner contours in the figure. For comparison, Fig. 1b shows the same plot based on all tropical cyclones. It is clear that float availability is lower than that in Fig. 1a, especially for relatively large time-space windows. This occurs because Argo floats are not uniformly distributed, and the weaker cyclones tend to cover a wider spatial range, including areas where floats are sparse. Thus, the current distribution of Argo floats is more useful for studying typhoons than weaker cyclones. In general, this kind of availability is certainly useful for statistical analysis of the ML variability under the influence of typhoons and is probably also useful in providing oceanic initial conditions for operational typhoon prediction.

4 ML background variability

Figure 2 shows the background ML variations within an Argo float repeating cycle, in the western North Pacific Ocean during the May–November typhoon season from 2000 to 2008. A total of more than 18,000 paired Argo profiles that are not influenced by typhoons (each pair from two successive profiles of the same float) are used to calculate the background ML variability. Even without the influence of a typhoon, the MLD can either deepen or shoal up to 60 m (Fig. 2a). Despite the large variance, the mean change in MLD is nearly zero at all latitudes, which indicates that, if the sample size is large enough, a statistical estimation of MLD variation induced by typhoons would not be seriously contaminated by the background variability.

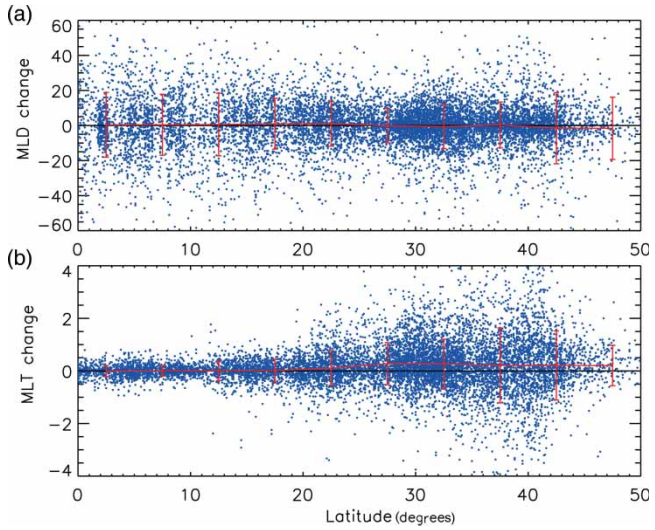

Fig. 2 Changes in (a) MLD (m) and (b) MLT (°C) observed in Argo profiles during one cycle (7–10 days) as a function of latitude in the typhoon season (May to November) without the influence of a tropical cyclone. The red curves are mean changes, and the red bars are the standard deviations of MLD and MLT at corresponding latitudes.

The background MLT variation is much larger at latitudes north of 25°N, and it can be as high as 4°C, even without the influence of a typhoon (Fig. 2b). At latitudes from 25°N to 50°N, the mean change in MLT over an Argo observation cycle is 0.2°C to 0.3°C during the months of May to November. Such a temperature increase is most likely related to the seasonal cycle. Therefore, when using Argo floats to study ocean-typhoon interactions at the synoptic scale, the seasonal information included in the Argo observation cannot be ignored.

To estimate the seasonal cycle of MLD and MLT, a regression model is applied to the background data at different latitude bands. For each 5-degree latitude box in the western North Pacific Ocean, 365 daily mean MLD or MLT values are fitted with seasonal harmonics in the form of $r(t_i) = a_0 + a_1 \cos(2\pi t_i/365) + a_2 \sin(2\pi t_i/365) + \varepsilon_i$ where $t_i = 1, 2, \ldots 365$ is the Julian day in each year, a_0 the long-term time mean, a_1 and a_2 the coefficients of the cosine and sine components of the Fourier representation of the climatological daily MLD and MLT, respectively. The coefficients a_0, a_1 and a_2 are estimated using linear regression minimizing $\Sigma\varepsilon^2$, where ε_i are the estimated residuals from the fit of the regression model. The characteristics of the harmonics can be represented in terms of amplitude $A = (a_1^2 + a_2^2)^{1/2}$ and phase $\varphi = \tan^{-1}(a_1/a_2)$ The statistical significance of the three estimated coefficients is evaluated using the F-test with the numerator and denominator degrees of freedom being 2 and 362, respectively (Anderson, 1971). This scale selection of the latitude box is based on a trade-off between the data availability and the consistency of the seasonal cycle.

Table 1 lists the seasonal cycle of the MLD and MLT at each latitudinal band. The statistical significance of the seasonal cycle for both the MLD and MLT at all latitudes is above

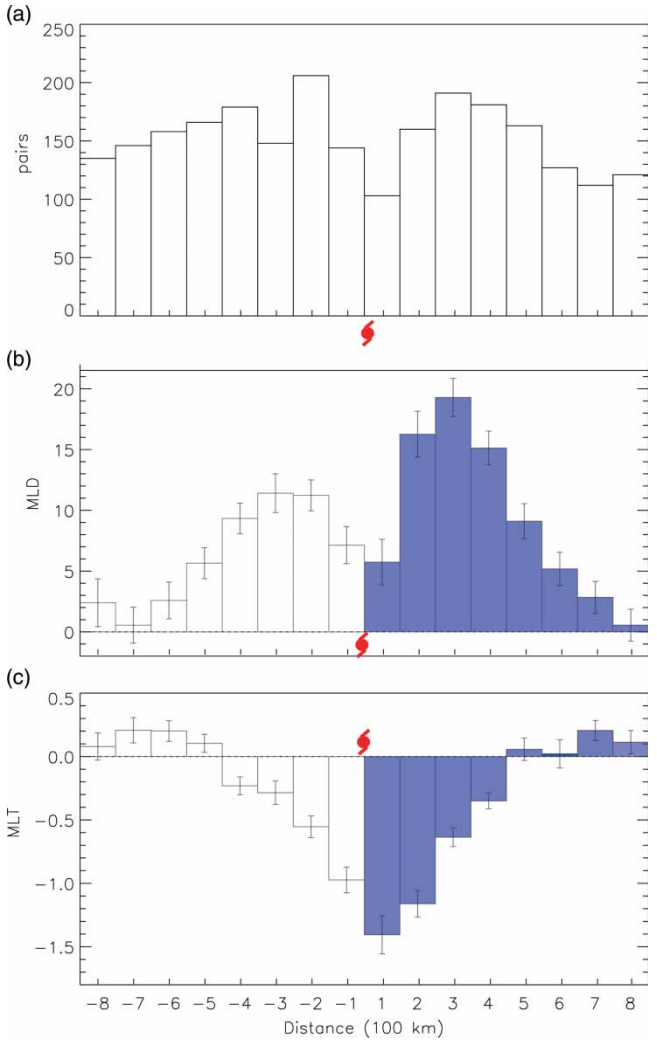

Fig. 3 Bar graphs of (a) number of Argo profile pairs, (b) MLD (m) change and (c) MLT (°C) change as a function of the distance from the typhoon centre. Negative (positive) distance means that the Argo profiles are located on the left (right) side of the typhoon track; the changes on the right of the track are in blue. Argo profiles within five days of a typhoon passage are counted. The error bars (black) in (b) and (c) are calculated as the standard deviation divided by the square root of the number of data pairs.

the 95% confidence level. At latitudes between 30°N and 50°N, in an Argo repeating cycle, the maximum seasonal evolution-related ML changes can reach 10 m for MLD and 1°C for MLT. The seasonal signal in Argo data can be removed by subtracting the seasonal cycle listed in Table 1. After the subtraction, the mean changes in MLD and MLT without the influence of a typhoon are close to zero at all latitudes. Then, it is appropriate to assume that the ML variations induced by a typhoon are unbiased by the background variability when the sample size is large enough. Nevertheless, considering the large ML background variations induced by mesoscale eddies and other processes, such as subinertial currents and diurnal variations, we still need to be careful with the ML variations deduced from a single Argo float.

TABLE 1. Seasonal cycle of MLD and MLT in the western North Pacific Ocean.

Latitude	MLD (m)	MLT (°C)
0°–5°N	$2.73\cos\left(\frac{2\pi t_i}{365}\right)+5.40\sin\left(\frac{2\pi t_i}{365}\right)+58.53$	$-0.12\cos\left(\frac{2\pi t_i}{365}\right)-0.18\sin\left(\frac{2\pi t_i}{365}\right)+29.36$
5°–10°N	$4.79\cos\left(\frac{2\pi t_i}{365}\right)+10.91\sin\left(\frac{2\pi t_i}{365}\right)+60.86$	$-0.19\cos\left(\frac{2\pi t_i}{365}\right)-0.45\sin\left(\frac{2\pi t_i}{365}\right)+28.99$
10°–15°N	$16.24\cos\left(\frac{2\pi t_i}{365}\right)+9.86\sin\left(\frac{2\pi t_i}{365}\right)+62.08$	$-0.52\cos\left(\frac{2\pi t_i}{365}\right)-0.66\sin\left(\frac{2\pi t_i}{365}\right)+28.54$
15°–20°N	$25.31\cos\left(\frac{2\pi t_i}{365}\right)+0.96\sin\left(\frac{2\pi t_i}{365}\right)+53.81$	$-1.15\cos\left(\frac{2\pi t_i}{365}\right)-0.94\sin\left(\frac{2\pi t_i}{365}\right)+28.09$
20°–25°N	$26.54\cos\left(\frac{2\pi t_i}{365}\right)-0.91\sin\left(\frac{2\pi t_i}{365}\right)+45.17$	$-1.74\cos\left(\frac{2\pi t_i}{365}\right)-1.95\sin\left(\frac{2\pi t_i}{365}\right)+26.91$
25°–30°N	$37.01\cos\left(\frac{2\pi t_i}{365}\right)+8.90\sin\left(\frac{2\pi t_i}{365}\right)+48.01$	$-2.06\cos\left(\frac{2\pi t_i}{365}\right)-3.50\sin\left(\frac{2\pi t_i}{365}\right)+24.43$
30°–35°N	$52.42\cos\left(\frac{2\pi t_i}{365}\right)+27.30\sin\left(\frac{2\pi t_i}{365}\right)+63.80$	$-1.91\cos\left(\frac{2\pi t_i}{365}\right)-4.43\sin\left(\frac{2\pi t_i}{365}\right)+21.95$
35°–40°N	$36.77\cos\left(\frac{2\pi t_i}{365}\right)+19.45\sin\left(\frac{2\pi t_i}{365}\right)+49.36$	$-3.01\cos\left(\frac{2\pi t_i}{365}\right)-5.23\sin\left(\frac{2\pi t_i}{365}\right)+17.43$
40°–45°N	$47.47\cos\left(\frac{2\pi t_i}{365}\right)+41.48\sin\left(\frac{2\pi t_i}{365}\right)+64.10$	$-2.53\cos\left(\frac{2\pi t_i}{365}\right)-5.28\sin\left(\frac{2\pi t_i}{365}\right)+10.93$
45°–50°N	$45.32\cos\left(\frac{2\pi t_i}{365}\right)+36.44\sin\left(\frac{2\pi t_i}{365}\right)+64.35$	$-1.85\cos\left(\frac{2\pi t_i}{365}\right)-4.04\sin\left(\frac{2\pi t_i}{365}\right)+6.88$

5 ML response to a typhoon

a ML Response to a Typhoon as a Function of Space and Time

After removing the seasonal signal, the Argo observations are used to study the upper ocean's response to typhoons in a statistical manner. Figure 3 presents the MLD and MLT responses to typhoons as a function of the distance to the typhoon centre, along with the number of data pairs used for the calculation. Significant deepening of the MLD and cooling of the MLT occur on both sides of the track. The magnitudes of the MLD deepening and MLT cooling decrease as the distance to the typhoon centre increases, except for a relatively small deepening near the typhoon centre as a result of the intense upwelling there. Significant deepening and cooling of the ML can reach about 400 km on both sides of the track. It is also interesting to note that the ML exhibits a striking asymmetrical response with more deepening and stronger cooling on the right side of the typhoon track. The rightward bias of the MLT is consistent with previous findings (Price, 1981; Lin et al., 2003; Walker et al., 2005). It occurs because the wind stress vector of a translating cyclone rotates clockwise with time on the right side of the track but anticlockwise on the left, which leads to a strong asymmetry in the ML velocity and thus in entrainment (Price, 1981).

The average changes in the MLD and MLT in response to typhoons are displayed in Fig. 4 as a function of the time before and after typhoon passage. The variation in both the MLD and MLT is very small before the arrival of a typhoon (negative time), which represents the background variability not accounted for by the seasonal cycle. The maximum MLD deepening occurs immediately after the passage of a typhoon, while the MLT cooling reaches its maximum one day later. This result is consistent with the model experiments of Bender et al. (1993) who showed that the rapid MLD deepening is caused by the combined effects of strong downwelling and entrainment at the front of the cyclone. Because the downwelling does not change the MLT and is followed by upwelling and continued vertical mixing, there should be a lag between the maximum MLT cooling and the maximum MLD deepening. It is also obvious from Fig. 4 that the MLT cooling can last for more than 10 days, while the MLD deepening seems to decay more rapidly. This is due to the fact that during the process of detrainment, the MLD shoals but the MLT does not have to change much. We will discuss this further in the last section.

b ML Response to Typhoons as a Function of Latitude and Translation Speed

Figure 5 shows the zonally averaged MLT and MLD responses to typhoons, along with the climatological mean MLD during the typhoon season, as a function of latitude. According to Price (1981) and Park et al. (2005), the ML response to typhoons should be stronger (weaker) where the initial MLD is shallower (deeper). This seems to be true at low latitudes, where the mean MLD is deep and the ML responses are rather weak. However, the maximum MLD deepening appears at latitudes around 20°N while the maximum MLT cooling occurs at latitudes from 20°N to 30°N, but

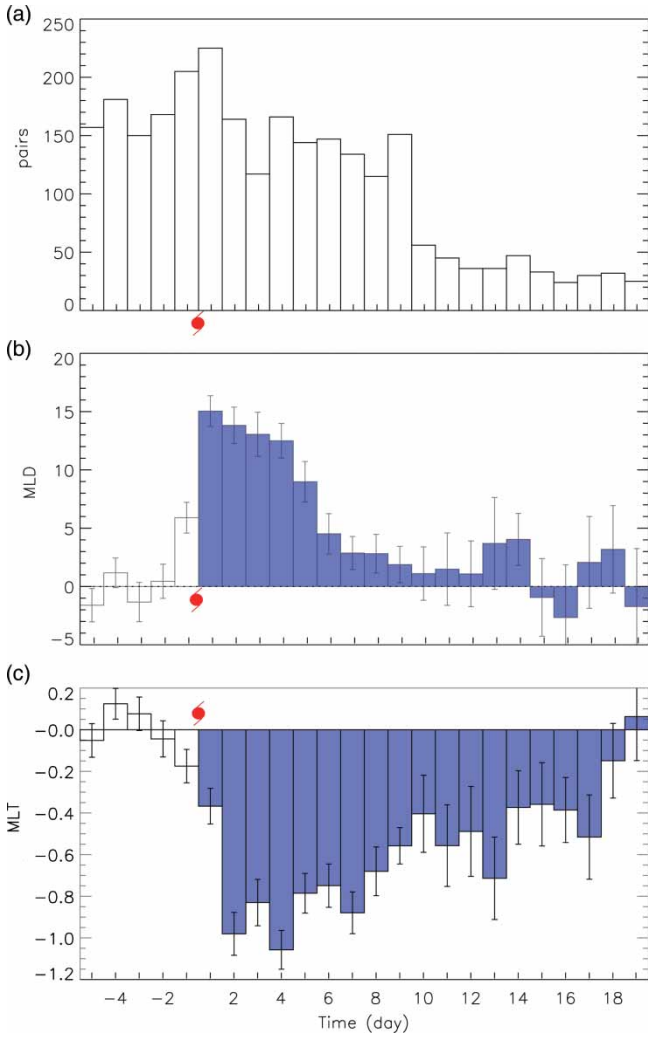

Fig. 4 As in Fig. 3 but as a function of time. Negative (positive) time means the Argo profiles observed before (after) the typhoon passage; the MLD and MLT changes after the typhoon passage are in blue. Argo profiles within 300 km of the typhoon track are counted. The error bars are shown in (b) and (c) in black.

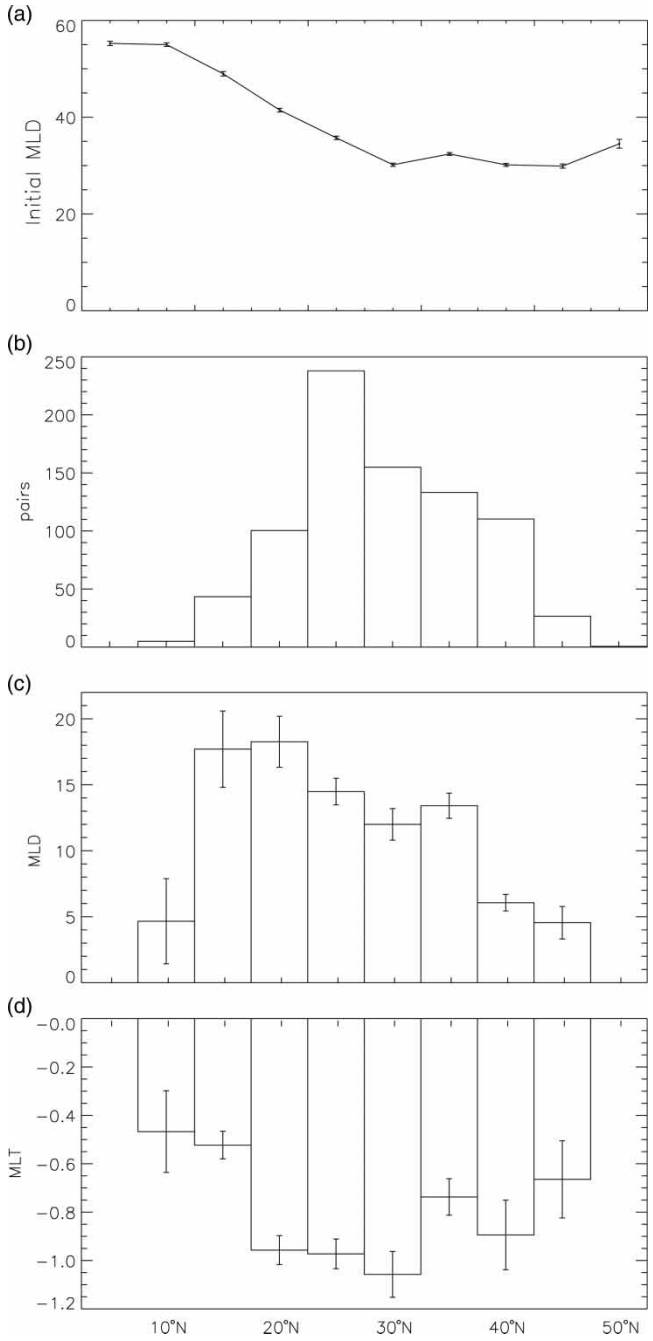

Fig. 5 (b)–(d) as in Fig. 3 (a)–(c) but as a function of latitude; (a) shows the climatological MLD during the typhoon season (May to November) without the influence of typhoons. Argo profiles within 5 days of a typhoon passage and 300 km from the typhoon track are counted. The error bars are shown in (c) and (d) in black.

there are no corresponding minima in the mean MLD at these latitudes. This suggests that the geographic difference in ML response to typhoons is determined not only by the mean state but that other factors must be taken into account. We will return to this after analyzing the effect of typhoon translation speed on the ML response.

Price (1981) pointed out that the upper ocean response strengthens significantly under slowly moving hurricanes ($\leq$4 m s^{-1}) and that after hurricane intensity the next most important factor in SST response is translation speed. In a case study of typhoon Kai-Tak, Lin et al. (2003) found that the SST drop was as large as 9°C because of the nearly stationary speed (0–1.4 m s^{-1}) of the cyclone. The average MLD and MLT responses to typhoons as a function of translation speed is presented in Fig. 6; the changes under slowly moving typhoons ($\leq$4 m s^{-1}) are in blue. Generally speaking, when typhoons move at speeds below 3 m s^{-1}, the ML shows a stronger deepening and cooling, with the latter being more prominent. This confirms that the ML response is indeed affected by the translation speed of typhoons. It is worth noting that there is no consistent pattern at higher speeds, indicating that the ML response is no longer controlled primarily by translation speed under these circumstances.

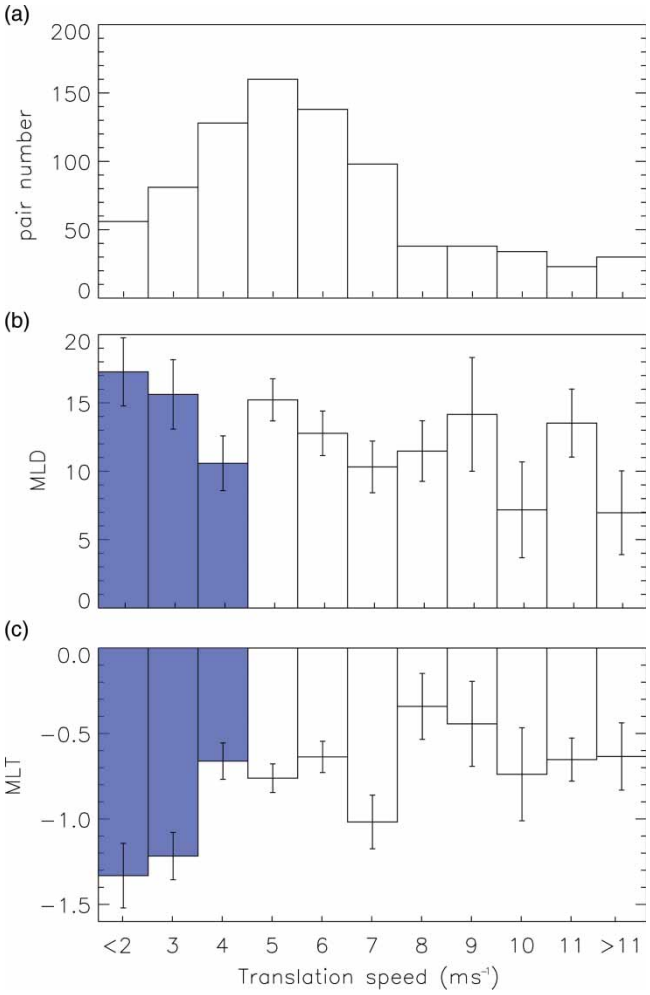

Fig. 6 As in Fig. 3 but as a function of typhoon translation speed. Argo profiles within 300 km of a typhoon track and within five days of a typhoon passage are counted. The columns in blue indicate translation speeds less than 4 m s^{-1}. The first column is for translation speeds less than 2 m s^{-1}, and the last column is for translation speeds greater than 11 m s^{-1}. The error bars are shown in (b) and (c) in black.

Because typhoon intensity and typhoon speed are the two main factors determining the upper ocean response to typhoons (Price, 1981), it is necessary to show the statistics of these two parameters (Fig. 7). In the western North Pacific Ocean, more than 40% of typhoons move at speeds less than 4 m s^{-1} (Fig. 7a), and they move more slowly at latitudes south of 30°N (Fig. 7b). Typhoons mostly intensify at latitudes between 10°N and 30°N, when they pass over the central region of the subtropical gyre (10°N–21°N) and over the warm features in the western North Pacific Ocean such as the southern eddy zone (21°N–26°N) and the Kuroshio (20°N–30°N) (Lin et al., 2008). Because both the slow translation speed and strong intensity of typhoons leads to larger ML deepening and cooling, the pronounced MLD deepening and cooling at subtropical and mid-latitudes (Fig. 5) should be caused, in part, by the strong, slow-moving typhoons at those latitudes.

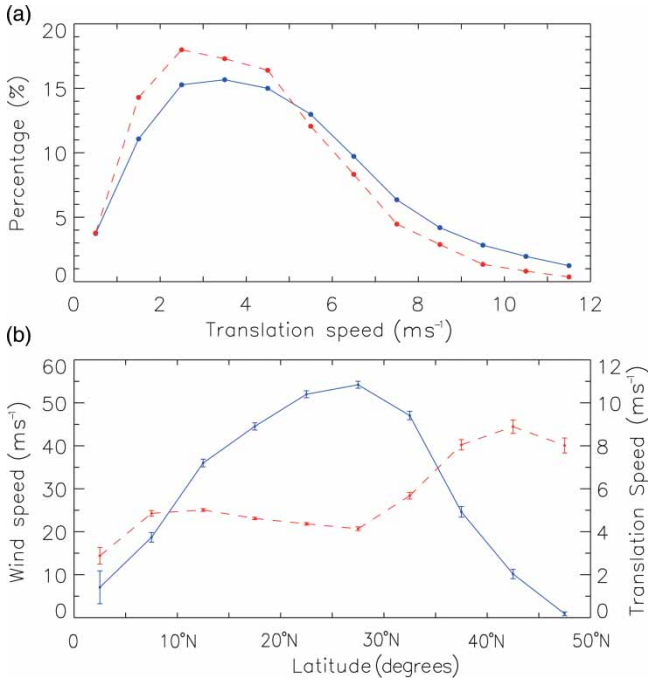

Fig. 7 (a) Percentage of typhoons moving at different speeds for the period 2000 to 2008. The solid curve shows all tropical cyclones and the dashed curve only typhoons. (b) The average wind speed of tropical cyclones (solid line) and typhoon translation speed (dashed line) as a function of latitude.

c ML Response to Typhoons as a Function of Initial Oceanic Conditions

Pre-existing mesoscale oceanic features have been shown to have a strong impact on the ML response to typhoons (Shay et al., 2000; Lin et al., 2008). When a typhoon approaches a cold-core cyclonic eddy, an extreme cooling response could be triggered (Zheng et al., 2008). On the other hand, when a typhoon passes a warm-core anticyclonic eddy, the MLT cooling is weak, and this lack of oceanic feedback often paves the way for typhoon intensification (Lin et al., 2008). To study the effects of pre-existing oceanic conditions, SSHAs occurring within seven days before the arrival of a typhoon are matched with the Argo floats recording the ML response. Figure 8 shows the pre-existing mesoscale SSHAs matched to Argo profiles in the western North Pacific Ocean. Negative features are located mainly in the region between 20°N and 40°N, while positive features cover a wider range, from the equator to 50°N.

Note that the distribution of SSHAs shown in Fig. 8 bears little resemblance to the well-known patterns of total eddy field in the western North Pacific Ocean. This is because the SSHA features shown here are only those closely related to typhoons (within 30 km of the Argo profiles used for ML response and within a week before typhoon passage). Also, not all of these SSHA features are real eddies although the same definition has been used in previous studies (Fu et al., 1994; Qiu, 1999; Shay et al., 2000; Lin et al., 2008). For convenience, we refer to negative (positive) SSHA features as cold-core

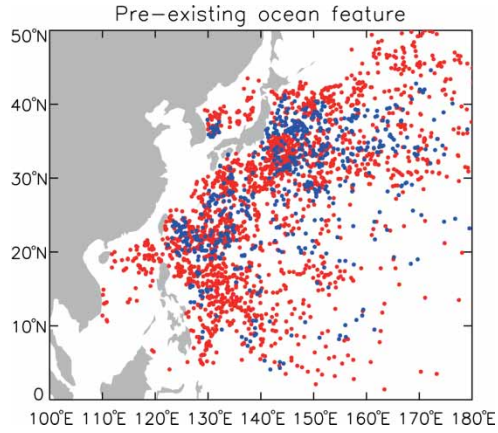

Fig. 8 Centre locations of pre-existing warm-core (red, SSHA >6 cm) and cold-core (blue, SSHA <–6 cm) circulation features before a typhoon passage.

(warm-core) cyclonic (anticyclonic) circulations, with the understanding that they are not necessarily closed eddies.

The dependence of the ML response on pre-existing oceanic condition is shown in Figs 9b and 9c. Again we see differential responses in MLD and MLT. It is clear that cold-core cyclonic circulation favours ML cooling while warm-core anticyclonic circulation favours ML deepening. This can be explained in terms of the different thermal structures of these mesoscale features (Fig. 9d). Within a cold-core circulation, the thermocline is elevated and the temperature gradient at the base of the ML is sharp, which makes entrainment of cold water from below more effective, leading to strong ML cooling without excessive deepening. Within a warm-core circulation, however, the thermocline is relatively deep and the temperature gradient at the base of the ML is weak, which makes it easy to deepen the MLD yet difficult to change the MLT. The different geographic distributions of the warm-core and

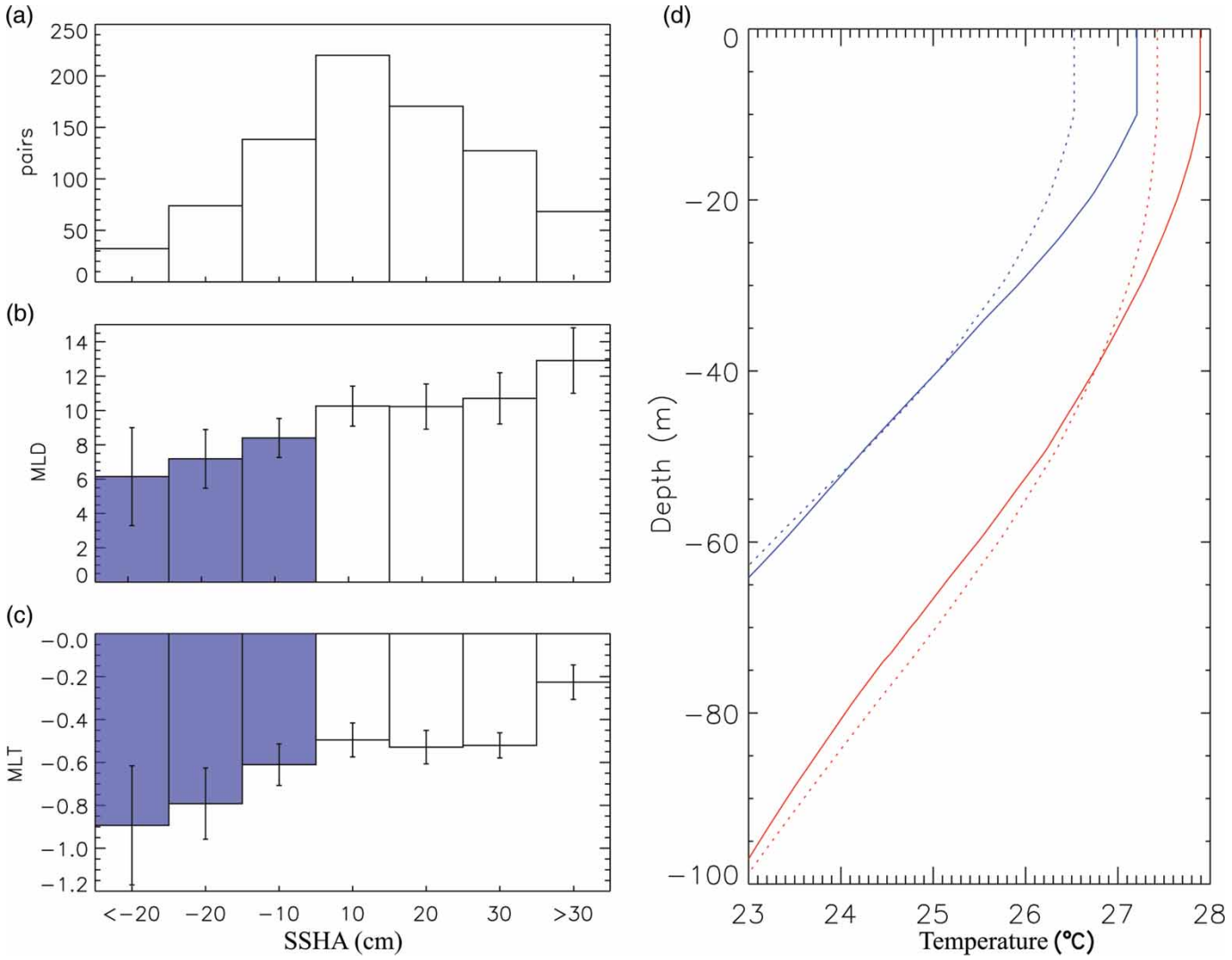

Fig. 9 (a)–(c) as in Fig. 3 (a)–(c) but as a function of pre-existing oceanic conditions. The columns in blue are for cold-core circulations and the white columns are for warm-core circulations. Argo profiles within 300 km of a typhoon track and five days of a typhoon passage are counted. A Student's *t*-test shows that the MLD and MLT changes under cold-core conditions are significantly different from those under warm-core conditions. (d) Composites of Argo temperature profiles for cold-core circulations (blue) and warm-core circulations (red). The solid (dotted) curves denote profiles before (after) a typhoon passage.

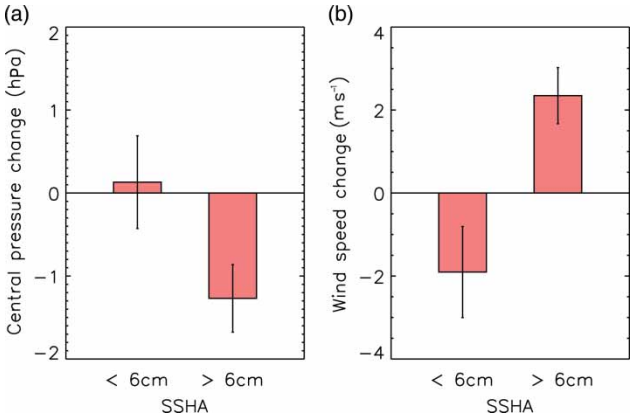

Fig. 10 Average changes in (a) central pressure and (b) maximum sustained wind speed one day after the eye of a typhoon passes over warm-core (SSHA >6 cm) and cold-core (SSHA <–6 cm) mesoscale features.

cold-core circulations (Fig. 8) may partly explain why the maximum MLD and MLT responses to typhoons occur in different latitude bands (Fig. 5).

The case study of tropical cyclones Katrina and Rita by Jaimes et al. (2011) supports the conclusions from our statistical analysis. They found that small MLT cooling over an anticyclonic eddy is a result of the combined effects of downwelling, turbulent entrainment over deep warm water and the vertical dispersion of near-inertial energy, while large MLT cooling over a cyclonic eddy is a combined result of the turbulent entrainment over strong stratification and the trapping of near-inertial energy that enhances the vertical thermal shear and mixing at the ML base.

Oceanic mesoscale features are important to the regulation of typhoon intensity (Lin et al., 2008; Jaimes et al., 2011). An additional analysis is performed to demonstrate this effect. Figure 10 shows the average changes in typhoon intensity (as measured by the central pressure as well as the maximum sustained wind speed) one day after the eye of a typhoon passes over warm-core or cold-core circulations. It is clear that, on average, typhoon strength weakens over a cold-core circulation, while it intensifies over a warm-core circulation. In relation to Fig. 9, this suggests that typhoon intensification over a warm-core circulation is associated with relatively large MLD deepening and small MLT cooling, while typhoon weakening over a cold-core circulation is associated with relatively small MLD deepening and large MLT cooling.

6 Summary and discussion

In this study, we performed a statistical analysis of the ML response to typhoons in the western North Pacific Ocean during the May–November typhoon season from 2000 to 2008, based on in situ Argo profiles, satellite altimetry and best-track typhoon data. After removing the seasonal cycle, the regional mean ML response to typhoons was quantified as a function of the distance from the typhoon centre, the time after typhoon passage, the geographic location, the translation speed of the typhoon, and the pre-existing patterns of oceanic circulation. Our analysis differs from previous studies of the same nature (e.g., Park et al., 2005; Liu et al., 2007) not only in the larger amount of Argo data used but also in the more complete set of parameters being explored.

The significance of this study is two-fold. On one hand, based on an unprecedented set of observational data, we have confirmed, on a robust statistical basis, some previous findings of the ML response to tropical cyclones, such as the rightward bias, the stronger response under slowly moving typhoons and the important effect of oceanic initial conditions. In fact, the latitudinal dependence of the ML response can be largely attributed to the combined effects of typhoon intensity, translation speed and initial MLD. On the other hand, our analysis reveals some significant differences between MLT and MLD changes induced by typhoons, including the delayed response of the MLT relative to the MLD, the longer restoring time of the MLT, and the tendency of pre-existing cold-core features to favour MLT cooling while warm-core features tend to favour ML deepening. These results have not been explicitly reported before and are worth more discussion here.

If the entrainment at the base of the ML was the only important process during the ML response to typhoons, one would expect the MLT and MLD changes to be in phase, with the maximum ML cooling and deepening occurring sometime after the passage of the typhoon centre. However, this simple picture is controversial. For instance, D'Asaro (2003) found, from neutrally buoyant floats, that the maximum ML cooling occurred before the passage of the typhoon eye, while the experiments of Bender et al. (1993) seem to imply that the maximum ML deepening should lead to maximum cooling. Our analysis shows a 1-day lag between the MLT and MLD maxima after the passage of the typhoon eye, which does not support the result of D'Asaro (2003), but favours the result of Bender et al. (1993) at least in a statistical sense. The reason is that the combined effects of strong downwelling and entrainment at the front of a typhoon cause rapid MLD deepening, and because the downwelling does not contribute to MLT cooling and is followed by upwelling and continued entrainment (both of which cause cooling), there should be a lag between the ML cooling and the deepening maximum.

Our analysis also indicates that, on average, the ML returns to its pre-storm depth about 5 days after the passage of a typhoon, while ML cooling recovers gradually over a period of more than 10 days. The reason for such disparity lies in the different effects of detrainment on the MLT compared to that of entrainment. During the process of ML recovery (detrainment), the MLD shallows as a result of the balance between solar heating and reduced wind forcing, but the MLT does not need to change much because the warm water that was mixed down during the earlier process of entrainment is left behind and cannot be "pulled back up." Therefore, the asymmetric effects of downwelling and upwelling on the MLT cause the rapid deepening and delayed

cooling in the initial stage of the ML response to typhoons, and similarly, it is the asymmetric effects of entrainment and detrainment on the MLT that are responsible for the prolonged restoring time of the MLT compared to that of the MLD after the passage of a typhoon.

As to the different impacts of pre-existing mesoscale oceanic features on the MLT and MLD responses to typhoons, we think that the explanation lies in the thermal structures of these features and the stratification below the ML. The results shown in Figs 9b and 9c seem a little puzzling at first. It is easy to understand the MLT response—the elevated and sharper thermocline under cold-core features leads to colder entrained water and thus stronger cooling, but why is the MLD response just the opposite? As evident in Fig. 9d, the initial MLD is about the same for warm-core and cold-core features, and thus for a given surface momentum input, the initial velocity jump across the base of the ML is about the same for both features, and the entrainment (ML deepening) is primarily determined by the density gradient there. Because the thermocline of a cold-core feature is sharper than a warm-core one, the former would favour ML cooling, and the latter would favour ML deepening.

In this study we have shown that the newly established observational network of Argo floats is useful for identifying the general characteristics of ML variability in response to typhoons in the western North Pacific Ocean. This is a pleasant surprise considering the fact that Argo was mainly conceived as a network for large-scale ocean circulation and climate studies. Because of the strong effect of oceanic feedback on typhoon intensification, and because of the difficulty in collecting in situ data under typhoon conditions by conventional means, the Argo floats have the potential to provide needed initial conditions for typhoon prediction. For that purpose, we need to increase the temporal and spatial resolutions of the Argo network in the breeding ground and along the main routes of typhoons. In particular, we should increase the number of Argo floats that have two-way communication capability, so that their sampling frequency and depth can be adjusted in real-time when typhoons arrive.

Acknowledgements

This work is supported by the National Basic Research Program (2007CB816005) and the National Science Foundation of China (40976018, 40730843). Funding to Q. Wu was also provided by the Talent Recruitment Project of the Second Institute of Oceanography (JR200801). The authors gratefully acknowledge the Japan Meteorological Agency for providing typhoon track data, Aviso for the SSHA data, and the China Argo Data Center for the Argo data. Helpful comments and criticisms from three anonymous reviewers are also greatly appreciated.

REFERENCES

Anderson, T. W. (1971). *The statistical analysis of time series*. Hoboken, NJ: John Wiley.

Bender, M. A., Ginis, I., & Kurihara, Y. (1993). Numerical simulations of tropical cyclone-ocean interaction with a high-resolution coupled model. *Journal of Geophysical Research*, *98,* 23245–23263.

D'Asaro, E. A. (2003). The ocean boundary layer below Hurricane Dennis. *Journal of Physical Oceanography*, *33,* 561–579.

de Boyer Montégut, C., Madec, G., Fisher, A. S., Lazar, A., & Iudicone, D. (2004). Mixed layer depth over the global ocean: An examination of profile data and a profile-based climatology. *Journal of Geophysical Research*, *109,* C12003. doi:10.1029/2004JC002378

de Boyer Montégut, C., Mignot, J., Lazar, A., & Cravatte, S. (2007). Control of salinity on the mixed layer depth in the world ocean: 1. General description. *Journal of Geophysical Research*, *112,* C06011. doi:10.1029/2006JC003953

Emanuel, K. (1999). Thermodynamic control of hurricane intensity. *Nature*, *401,* 665–669.

Fu, L. L., Christensen, E. J., Yamarone, C. A., Lefebvre, M., Menard, Y., Dorrer, M., & Escudier, P. (1994). TOPEX/POSEIDON mission overview. *Journal of Geophysical Research*, *99,* 24369–24381.

Gould, J. (2005). From swallow floats to Argo—the development of neutrally buoyant floats. *Deep Sea Research, Part II*, *52,* 529–543.

Grodsky, S. A., Carton, J. A., & Liu, H. (2008). Comparison of bulk sea surface and mixed layer temperatures. *Journal of Geophysical Research*, *113,* C10026. doi:10.1029/2008JC004871

Iwasaka, N., Kobashi, F., Kinoshita, Y., & Ohno, Y. (2006). Seasonal variations of the upper ocean in the western North Pacific observed by an Argo float. *Journal of Oceanography*, *62,* 481–492.

Jaimes, B., Shay, L. K., & Halliwell, G. R. (2011). The response of quasi-geostrophic oceanic vortices to tropical cyclone forcing. *Journal of Physical Oceanography*, *41,* 1965–1985.

Lin, I., Liu, W. T., Wu, C., Wong, G.T. F., Hu, C., Chen, Z., … Liu, K. (2003). New evidence for enhanced ocean primary production triggered by tropical cyclone. *Geophysical Research Letters*, *30,* 1718. doi:10.1029/2003GL017141

Lin, I.-I., Wu, C.-C., Pun, I.-F., & Ko, D.-S. (2008). Upper ocean thermal structure and the western North Pacific category-5 typhoons. Part I: Ocean features and category-5 typhoons intensification. *Monthly Weather Review*, *136,* 3288–3306.

Lin, I.-I., Pun, I.-F., & Wu, C.-C. (2009). Upper ocean thermal structure and the western North Pacific category-5 typhoons part II: Dependence on translation speed. *Monthly Weather Review*, *137,* 3744–3757.

Liu, Z., Xu, J., Zhu, B., Sun, C., & Zhang, L. (2007). The upper ocean response to tropical cyclones in the northwestern Pacific analyzed with Argo data. *Chinese Journal of Oceanology and Limnology*, *25.* doi:10.1007/s00343-007-0123-8

Park, J. J., Park, K. A., Kim, K., & Youn, Y. H. (2005), Statistical analysis of upper ocean temperature response to typhoons from ARGO floats and satellite. *Geoscience and Remote Sensing Symposium*, IGARSS '05 Proceedings. 2005 IEEE International, 25–29 July 2005, Seoul, Korea, Vol. 4, 2564–2567.

Price, J. F. (1981). Upper ocean response to a hurricane. *Journal of Physical Oceanography*, *11,* 153–175.

Qiu, B. (1999). Seasonal eddy field modulation of the North Pacific Subtropical Countercurrent: TOPEX/POSEIDON observations and theory. *Journal of Physical Oceanography*, *29,* 1670–1685.

Roemmich, D., & Gilson, J. (2001). Eddy transport of heat and thermocline waters in the North Pacific: A key to interannual/decadal climate variability? *Journal of Physical Oceanography*, *31,* 675–687.

Roemmich, D., Riser, S., Davis, R., & Desaubies, Y. (2004). Autonomous profiling floats: Workhorse for broadscale ocean observations. *Marine Technology Society Journal*, *38,* 31–39.

Shay, L. K., Goni, G. J., & Black, P. G. (2000). Effects of a warm oceanic feature on Hurricane Opal. *Monthly Weather Review*, *128,* 1366–1383.

Siswanto, E., Ishizaka, J., Morimoto, A., Tanaka, K., Okamura, K., Kristijono, A., & Saino, T. (2008). Ocean physical and biogeochemical responses to the passage of Typhoon Meari in the East China Sea observed from Argo float and multiplatform satellites. *Geophysical Research Letters*, *35*(15), L15604. doi:10.1029/2008GL035040

Stramma, L., Cornillon, P., & Price, J. F. (1986). Satellite observations of sea surface cooling by hurricanes. *Journal of Geophysical Research*, *91*(C4), 5031–5035.

Wada, A., & Chan, J.C. L. (2008). Relationship between typhoon activity and upper ocean heat content. *Geophysical Research Letters*, *35,* L17603. doi:10.1029/2008GL035129

Wada, A., Niino, H., & Nakano, H. (2009). Roles of vertical turbulent mixing in the ocean response to Typhoon Rex (1998). *Journal of Oceanography, 65,* 373–396.

Walker, N. D., Leben, R. R., & Balasubramanian, S. (2005). Hurricane forced upwelling and chlorophyll a enhancement within cold-core cyclones in the Gulf of Mexico. *Geophysical Research Letters*, *32,* L18610. doi:10.1029/2005GL023716

Withee, W. G. & Johnson, A. (1976). Data report: Buoy observations during Hurricane Eloise (September 19 to October 11, 1975). U.S. Department of Commerce, NOAA, NSTL station, Mississipi.

Yasuda, I., Okuda, K., & Hirai, M. (1992). Evolution of a Kuroshio warm-core ring—Variability of the hydrographic structure. *Deep Sea Research*, *39,* 131–161.

Zheng, Z.-W., Ho, C.-R., & Kuo, N.-J. (2008). Importance of pre-existing oceanic conditions to upper ocean response induced by Super Typhoon Hai-Tang. *Geophysical Research Letters*, *35,* L20603. doi:10.1029/2008GL035524